Adaptive Eccentricity Compensation

Carlos Canudas de Wit and Laurent Praly

***Abstract*—This paper is devoted to the problem of rejecting oscillatory position-dependent disturbances with unknown frequency and unknown amplitude. The considered disturbances are here assumed to be produced by eccentricity in mechanical systems and drives. Most of the previous works on eccentricity cancellation assume a *time-depending* oscillation, we instead assume that the oscillatory disturbance is *position-dependent*. This leads us to formulate and to globally solve the adaptive cancellation problem using a velocity-dependent internal model of the eccentricity. The proposed control design results in an asymptotically globally stable adaptive eccentricity compensator (AEC). An apparatus with rolling eccentricity has been build to test the controller. The paper presents a serial of experimental results showing the improvements of this controller. Also a comparative study with a simple pororsional integral (PI) regulator is presented.**

***Index Terms*—Adaptive compensation, eccentricity sinusoidal disturbance rejection.**

I. Introduction

We consider systems of the form

$$J\dot{v} = u + d(x); \quad v = \dot{x} = \frac{dx}{dt} \tag{1}$$

where x is the system angular position, J is the inertia, u is the control input and $d(x)$ is the position-dependent oscillatory disturbance defined as

$$d(x) = \Lambda \cos(\omega x + \Phi). \tag{2}$$

It is assumed that the amplitude Λ, the dimensionless frequency ω, and the phase Φ of the disturbance d are unknown. The problem considered here is thus to cancel the effect of the disturbance d in the system (1).

This type of problem arises as a consequence of eccentricity in many mechanical systems where the center of rotation does not corresponds with its geometric center. This is typically the case on drives with magnetic bearings. It also arises in systems with friction where the contact forces change as a function of the position x.

The dependency on position of $d(x)$ can be visualized in the following scenarios. It is known that the friction forces depends on the normal force acting between two surfaces. Inaccuracies in the geometric position of the rotating axis of a rolling mill (eccentricity), will produce position dependent disturbances. In gear boxes, friction will vary as a function of the effective surface in contact with the gear's teeth. The two-dimensional rolling and spinning friction causes in ball bearings the frictional torque to be dependent on both position and velocity. Fig. 1 shows some of these examples.

Many of the existing works consider d not as a position function, but as a time-dependent exogenous signal, of the form

$$d(t) = \Lambda \cos(\omega t + \Phi). \tag{3}$$

In the previous mentioned system this hypothesis is only valid if we assume that the system is operating and regulated, at constant velocity v_d so that $x(t)$ becomes proportional $t \cdot v_d$. Disturbances of the form (3) have been considered in problems such as active noise and vibration control. The noise $d(t)$ is thus assumed to be generated by the rotating machinery and transmitted through the sensor path. Examples rate from engine noise in turboprop aircraft [5] to ventilation noise in HVAC system [6], passing through engine noise in automobiles [10].

The proposed solutions resort to "standard" adaptive algorithms if the frequency ω is assumed to be known [2]. Repetitive control has also been used to compensate eccentricity in rolling [7]. For the general case where both amplitude and frequency are unknown, some approaches based on the *phase-lock loop* principle has been proposed [1], but without proof of stability. When formulating this problem in the time-domain, the main difficulty to show global stability properties of the adaptive algorithms comes from the fact that the unknown parameters appear nonlinearly in the (3).

When the system operates under time-varying velocity profiles, ω in (3) becomes time-dependent generating a signal $d(t)$ with a large frequency contain. The position dependent disturbance model (2) is thus better adapted for those cases.

In this paper, we present a globally stable adaptive algorithm that solves the above mentioned problem. For this, we use a velocity-dependent state-space representation for $d(x)$. An adaptive observer is thus designed ensuring global asymptotic stability. The observer is constructed such that can be used in open loop (for predicting oscillatory disturbances in view of diagnostic applications), or in closed loop (to compensate for the eccentricity effect). The properties of the algorithm are invariant with respect to the operating velocity v.

The second part of the paper describes the experimental evaluation of AEC-controller tested on a special purpose apparatus that exhibits rolling eccentricity. The performance of the proposed controller is evaluated with several velocity signal profiles (i.e., constant, time-varying), and finally we present a comparison with the standard proportional integral (PI) controller.

Manuscript received October 28, 1998; revised May 2, 1999. Recommended by Associate Editor, M. Bodson.

C. Canudas de Wit is with the Laboratoire d'Automatique de Grenoble, ENSIEG-INPG, 38402 St. Martin d'Hères, France (e-mail: canudas@lag.ensieg.inpg.fr).

L. Praly is with Ecole des mines de Paris, Centre Automatique, 77305 Fontainebleau, France (e-mail: praly@cas.ensmp.fr).

Publisher Item Identifier S 1063-6536(00)05747-X.

1063–6536/00$10.00 © 2000 IEEE

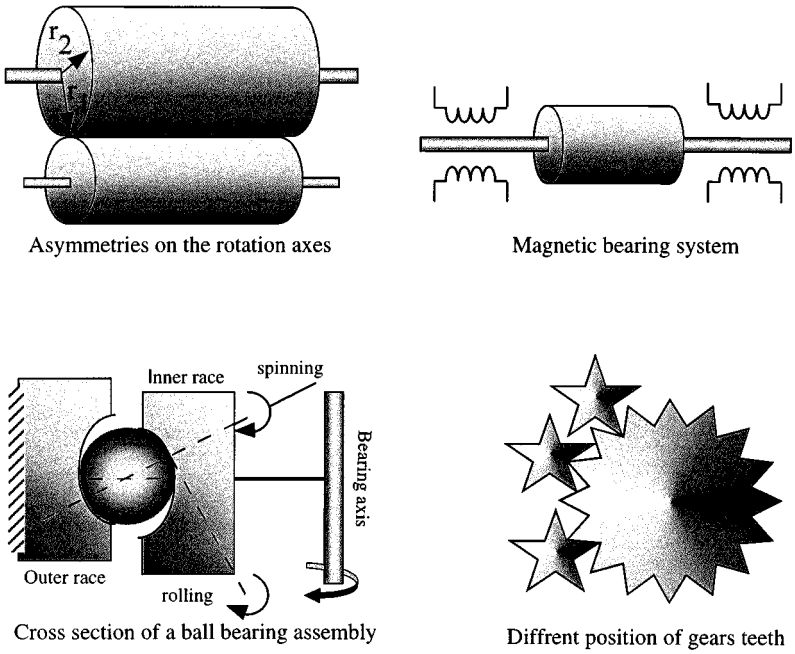

Fig. 1. Examples of systems where disturbances $d(x)$ are positions-dependent and may produce eccentricity: the upper left figure shows an example of a systems where the shear force acting on the surface of contact may vary as a function of the joint angle positions, due to eccentricity on the axis of rotation if $r_1 \neq r_2$. In the system with magnetic bearing (upper right), the geometric axis of the cylinder does not coincide with the axis of rotation due to unbalanced masses distribution. The left lower figure shows the spinning and rolling resistances induce a variation on the effective area of contact as a function of the inner race position and in the right lower figure this variation is due to the relative position of the gears teeth.

II. Control Design

In this section we formulate the internal model for the disturbance d, and then we present the control design that includes the adaptive observer. We also present the stability properties of such a design.

Internal model for d: Let $z = [z_1, z_2]^T$, be defined as

$$z_1 = \Lambda \cos(\omega x + \Phi) \tag{4}$$

$$z_2 = -\frac{\Lambda}{\omega} \sin(\omega x + \Phi) \tag{5}$$

this gives the following state-space representation for d:

$$\dot{z}_1 = v\omega^2 z_2 \tag{6}$$

$$\dot{z}_2 = -v z_1 \tag{7}$$

$$d = z_1. \tag{8}$$

The above set of equation describes the velocity-dependent state-space (internal) model for the eccentricity.

Observer structure: These equations together with system equation (1) suggest the following observer structure:

$$J\dot{\hat{v}} = u + \hat{z}_1 - k_0(\hat{v} - v) \tag{9}$$

$$\dot{\hat{z}}_1 = v\hat{\theta}\hat{z}_2 - k_1(\hat{v} - v) - k_1 s(v_d - v) \tag{10}$$

$$\dot{\hat{z}}_2 = -v\hat{z}_1 \tag{11}$$

where $\hat{\theta}$ is an estimate for $\theta = \omega^2$ (the adaptation law for $\hat{\theta}$ will be designed latter). $\hat{v}$ is an estimated for v needed to design our full-order observer[1]. k_0, and k_1 are positive constants. The variable s is used to select between two possible operation modes: an eccentricity predictor if $s = 0$, or $s = 1$ if the observer is to be used in closed loop as a eccentricity compensator. $v_d(t)$ is the velocity time-profile to be followed.

Error equations: We consider the problem of tracking the desired velocity $v_d(t)$ supposed to be bounded and continuous as well as its derivative. To this aim we define the adaptive eccentricity control (AEC) control as

$$u = J\dot{v}_d - k_v(v - v_d) - s \cdot \hat{z}_1 \tag{12}$$

with $k_v > 0$. $\hat{z}_1$ is given by the observer above, and the adaptive law to be derived.

Introducing the following error definitions $\tilde{v} = \hat{v} - v$, $e = v_d - v$, $\tilde{z}_1 = \hat{z}_1 - z_1$, $\tilde{z}_2 = \hat{z}_2 - z_2$, $\tilde{\theta} = \hat{\theta} - \theta$, we have that the closed-loop error equations are

$$J\dot{e} = -k_v e + (s\hat{z}_1 - z_1) \tag{13}$$

$$J\dot{\tilde{v}} = -k_0\tilde{v} + \tilde{z}_1 \tag{14}$$

$$\dot{\tilde{z}}_1 = v\theta\tilde{z}_2 - \tilde{v}k_1 - sk_1 e + v\tilde{\theta}\hat{z}_2 \tag{15}$$

$$\dot{\tilde{z}}_2 = -v\tilde{z}_1. \tag{16}$$

Adaptation law: The adaptation law is derived from the following analysis. Introduce V as

$$V = \frac{1}{2}\left[Jk_1(\tilde{v}^2 + se^2) + \tilde{z}_1^2 + \omega^2\tilde{z}_2^2 + \gamma^{-1}\tilde{\theta}^2\right]$$

and this gives

$$\dot{V} = -k_0k_1\tilde{v}^2 - sk_vk_1e^2 + k_1\tilde{z}_1(s \cdot e + \tilde{v}) + \tilde{z}_1(v\hat{\theta}\hat{z}_2 - k_1\tilde{v} - sk_1e + v\tilde{\theta}\hat{z}_2) - v\theta\tilde{z}_2\tilde{z}_1 + \tilde{\theta}\dot{\hat{\theta}}\gamma^{-1} \tag{17}$$

$$= -k_0k_1\tilde{v}^2 - sk_vk_1e^2 + \tilde{\theta}[v\hat{z}_2\tilde{z}_1 + \gamma^{-1}\dot{\hat{\theta}}] \tag{18}$$

[1]It is also possible to design a reduced-order observer, but this results in an observer that is highly noise sensitive. Instead, we have introduced in this paper the full-order observer that has better noise rejection characteristics.

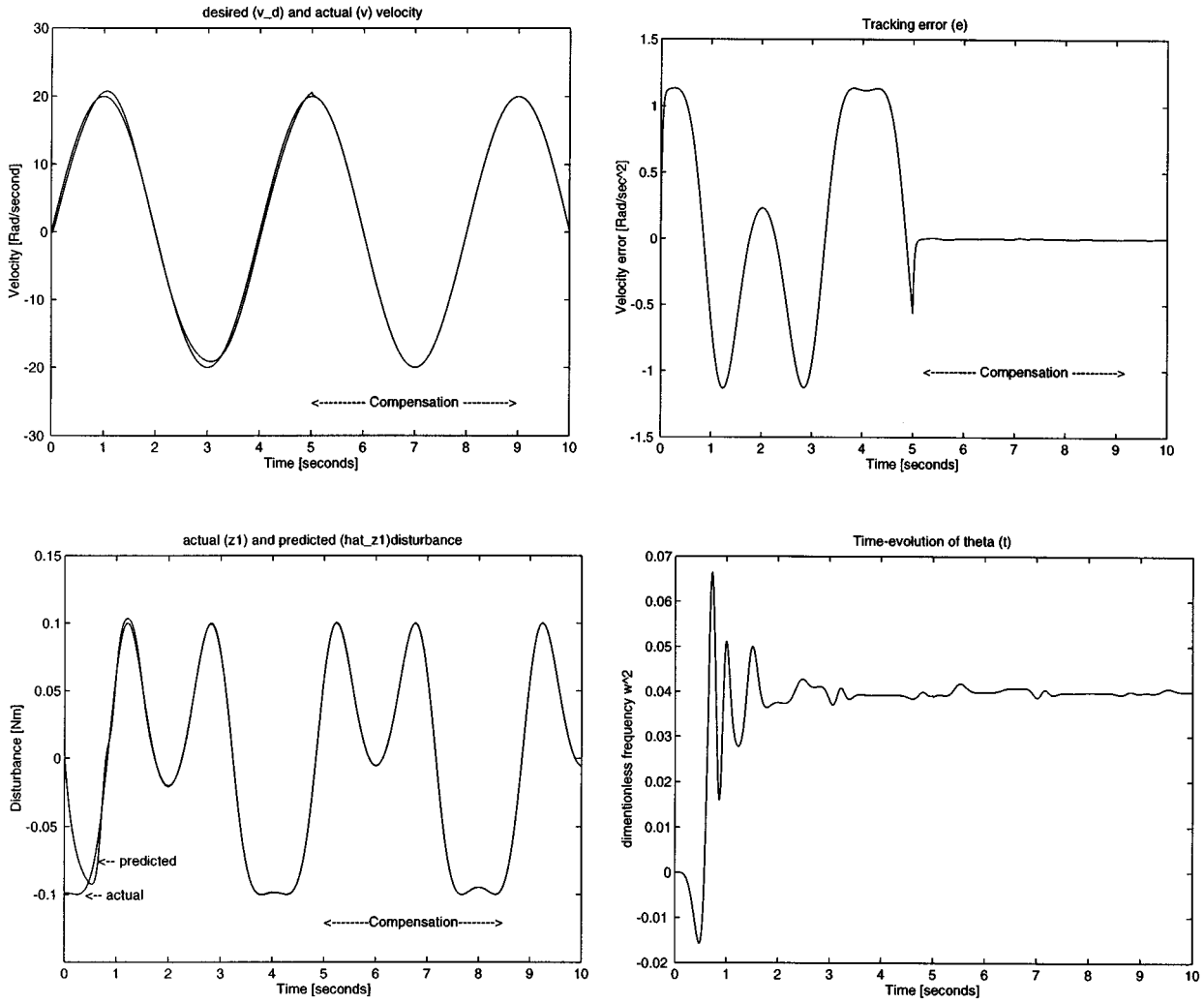

Fig. 2. Simulation results with $v_d = 20\cos(\pi/2)t$. Upper left: desired (v_d) and closed-loop system (v) velocity. Upper right: Velocity tracking error time profile. Lower left: Actual (z_1) and predicted $(\hat{z}_1)$ disturbance. Lower right: Time-evolution of $\hat{\theta}(t)$.

which suggests to define $\dot{\hat{\theta}}$ as

$$\dot{\hat{\theta}} = -\gamma v \hat{z}_2 \tilde{z}_1 \tag{19}$$

which cancels the term between the square brackets, resulting in in a seminegative function $\dot{V} \leq 0$, i.e.,

$$\dot{V} = -k_0 k_1 \tilde{v}^2 - s k_v k_1 e^2 \leq 0.$$

Standard arguments along the Barlabat's lemma can be here applied to conclude that $\tilde{v}$, e, and $\tilde{z}_1$tend asymptotically to zero, while all the internal signal of the system remain bounded.

The representation of the adaptation law (19) is appropriate for analysis. But it cannot be implemented directly in this way unless the system acceleration, is assumed to be measurable (note that $\tilde{z}_1 = \hat{z}_1 + u - J\dot{v}$). Alternatively, we can introduce a change of coordinates in $\hat{\theta}$ and then show that measurement of $\dot{v}$ is not needed.

To this aim, note that $\dot{\hat{\theta}}$ can be rewritten as

$$\dot{\hat{\theta}} = -\gamma v \hat{z}_2 [\hat{z}_1 + u - J\dot{v}] \tag{20}$$

$$= -\gamma v \hat{z}_2 (\hat{z}_1 + u) + \gamma J \hat{z}_2 v \dot{v} \tag{21}$$

$$= -\gamma v \hat{z}_2 (\hat{z}_1 + u) + \frac{1}{2}\gamma J \hat{z}_2 \frac{d}{dt}\{v^2\} \tag{22}$$

$$= -\gamma v \hat{z}_2 (\hat{z}_1 + u) + \frac{1}{2}\gamma J \left[v^3 \hat{z}_1 + \frac{d}{dt}\{\hat{z}_2 v^2\} \right] \tag{23}$$

$$= -\gamma v \left[\hat{z}_2 (\hat{z}_1 + u) - \frac{J}{2} v^2 \hat{z}_1 \right] + \frac{1}{2}\gamma J \frac{d}{dt}\{\hat{z}_2 v^2\} \tag{24}$$

or equivalent

$$\frac{d}{dt}\left\{ \hat{\theta} - \frac{J\gamma}{2}\hat{z}_2 v^2 \right\} = -\gamma v \left[\hat{z}_2 (\hat{z}_1 + u) - \frac{J}{2} v^2 \hat{z}_1 \right].$$

Defining the new variable $\hat{\varphi}$ as

$$\hat{\varphi} = \hat{\theta} - \frac{J\gamma}{2} v^2 \hat{z}_2 \tag{25}$$

we have

$$\dot{\hat{\varphi}} = -\gamma v \left[\hat{z}_2 (\hat{z}_1 + u) - \frac{J}{2} v^2 \hat{z}_1 \right].$$

The complete set of equations defining the AEC controller can thus be rewritten in the new set of coordinates $(\hat{v}, \hat{z}, \hat{\varphi})$ only as a function of the velocity, i.e.,

$$u = J\dot{v}_d - k_v(v - v_d) - s\hat{z}_1 \tag{26}$$

$$J\dot{\hat{v}} = u + \hat{z}_1 - k_0(\hat{v} - v) \tag{27}$$

$$\dot{\hat{z}}_1 = v\left[\hat{\varphi} + \frac{J\gamma}{2}v^2\hat{z}_2\right]\hat{z}_2 - k_1(\hat{v} - v) - sk_1(v_d - v) \tag{28}$$

$$\dot{\hat{z}}_2 = -v\hat{z}_1 \tag{29}$$

$$\dot{\hat{\varphi}} = -\gamma v\left[\hat{z}_2(\hat{z}_1 + u) - \frac{J}{2}v^2\hat{z}_1\right]. \tag{30}$$

The following theorem summarizes our main result.

Theorem 1: Consider the system (1)–(2). Consider the dynamic feedback defined by the equation set (26)–(30). Let the control gains $k_v > 0, k_0 > 0, k_1 > 0, \gamma > 0$. Then all the internal signal of the system are bounded and the velocity tracking error e and the eccentricity prediction error $\tilde{z}_1$ tend asymptotically to zero.

III. Simulation Results

We present in this section a simulated example, with the system (1), and the AEC controller. Values used in simulations were as follows.

- *System parameters* $J = 0.0022$, $\Lambda = 0.1$ (Nm), $\omega = 0.2$ (Rad/m), $\Phi = 3$ (Rad).
- *Controller gain* $k_v = J \cdot 40$.
- *Observer* $k_0 = 1, k_1 = 5$.
- *Adaptation law* $\gamma = 5$.

First simulations where performed with a oscillatory velocity profile $v_d = 20\cos(\pi/2)t$. The first 5 s presented in the simulations do not use the adaptive compensation scheme (although the adaptation mechanism is active since $t \geq 0$, i.e., $s = 0$). Eccentricity compensation is activated $(s = 1)$ during $t \in [5, 10]$. The upper left Fig. 2, shows the velocity desired profile, and the closed-loop velocity. Substantial improvements can be observed with eccentricity compensation (see tracking error in the upper right of Fig. 2).

The disturbance $d = z_1$ and the estimated disturbance $\hat{z}_1$ are shown in the lower left of Fig. 2. A fast convergence of the eccentricity estimated to its true value is obtained. Finally the lower rigtht Fig. 2 gives the time-evolution of the estimated parameter $\hat{\theta}$. It can be observed that $\hat{\theta}$ converge to its true value, i.e., $\hat{\theta} \to 0.04$.

IV. Experimental Results

This section describes the experimental evaluation of AEC-controller. We first provide a description of the apparatus used for the experiments, then we evaluate the AEC performance with several velocity signal (constant, time-varying), and finally we present a statistic comparison between the AEC and the standard PI controller. More detailed description of the real-time system used for these experiments, as well as additional experiments, can be found in [8].

A. Description of the Experimental Setup

The schematic view of the aparatus build to study eccentricity is shown in Fig. 3. The lateral view in Fig. 3 shows, from right to left, the motor drive [0.5 KW], the gear box (with a reduction ratio of $n = 15.5$), the load, and the wheel used to produce the eccentricity effects. The front view shows the details of this mechanism. The load cylinder of inertia J_l is driven by the motor of inertia J_m. On the top of it, we have placed a rotating wheel (with neglected inertia), constrained by the force F_N. The rotation wheel's center is set to be different from its geometric center. The contact pressure at the point where the wheel radius is equal to R, is larger than the contact pleasure at the point of radius r, since $R > r$. This produces an eccentricity effect changing the normal force acting on the wheel-to-cylinder contact surface. This variation is then transmitted to the motor shaft via the gear box. The additional normal force, at the load side, induced by this mechanism can thus be modeled as

$$F_N^{\text{load}} = F_N\left[1 + k_S\frac{R - r}{2}\cos(\bar{\omega}x_l + \Phi)\right] \tag{31}$$

where x_l is the load angle (Rad), which is related to the motor angle position as $x = nx_l$ ($n = 15.5$ is the reduction ratio). k_S (1/m) is a constant capturing the linear part of the rubber o-ring deformation. Φ, is the phase shift, and $\bar{\omega}$ describes the dimensionless eccentricity frequency. This frequency is defined as the ratio between the the cylinder's radius, and the wheel's average radius, i.e.,

$$\bar{\omega} = \frac{2R_0}{r + R}.$$

This value, although computable here in our set up, will be assumed to be unknown as may be the case in many applications with complicated mechanisms. Since the inertia of the wheel of negligible when compared to the load cylinder, other dynamic effects of the wheel will not be considered.

The model for the motor drive under this setup is given as

$$J\dot{v} = u - F_m; \quad v = \dot{x} = \frac{dx}{dt} \tag{32}$$

where x (Rad) is the motor angular position, $J = J_m + J_l/n^2$ (Nm/s^2) is the total system inertia (motor plus load), u (Nm) is the control torque input, and F_m (Nm) is the motor friction torque at the ball bearings. F_m depends, among other factors, on the normal force variations induced by the eccentric wheel, and it is modeled as

$$F_m = \left[F_{Nm} + F_N^{\text{load}}\right]\nu(\eta, \dot{\eta}, v) \tag{33}$$

$$\dot{\eta} = v - \frac{\bar{\sigma}_0|v|}{\mu_0}\eta \tag{34}$$

with

$$\nu(\eta, \dot{\eta}, v) \triangleq \bar{\sigma}_0\eta + \bar{\sigma}_1\dot{\eta} + \bar{\sigma}_2 v.$$

where F_{Nm} is the average normal force on the ball bearings, F_N^{load}, is as defined in (31), the parameters $\bar{\sigma}_i$ are the friction parameters associated to the LuGre friction model (see [3]).

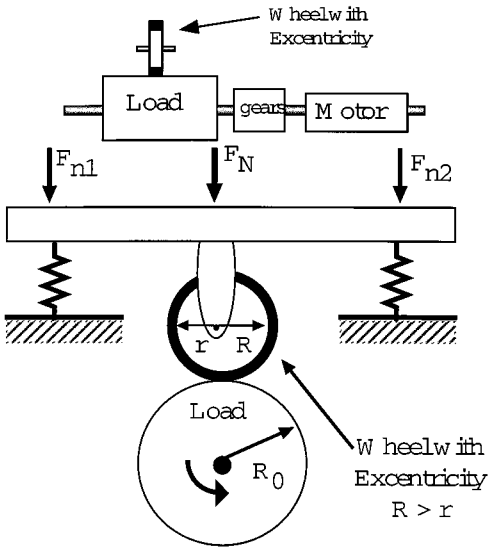

Fig. 3. Schematic (top) lateral view of the experimental setup to study eccentricity (bottom) front view.

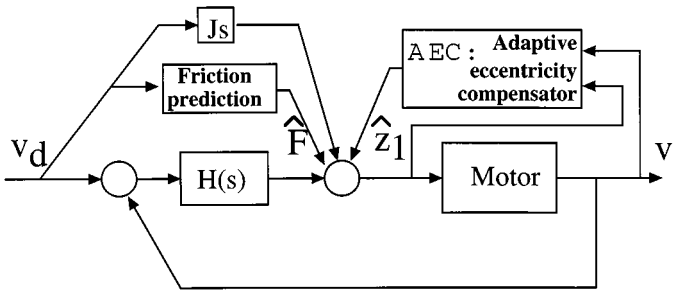

Fig. 4. Control block scheme of the adaptive eccentricity compensator (AEC) with feedforward friction compensation.

TABLE I
MOTOR, FRICTION, AND LOAD PARAMETERS

Friction parameters	Motor parameters	Wheel & cylinder characteristics
$F_C = 0.38\ [Nm]$	$J_m = 0.00196\ [Kg/m^2]$	$R_0 = 6\ [cm]$
$F_S = 0.42\ [Nm]$	$J_l = 0.0125\ [Kg/m^2]$	$R = 2.1\ [cm]$
$v_0 = 0.01\ [rad/sec]$	$J = 0.0022\ [Kg/m^2]$	$r = 1.9[cm]$
$\sigma_0 = 260.0\ [Nmsec/rad]$	$K_t = 0.352\ [Nm/Amp]$	
$\sigma_1 = 0.6\ [Nm/rad]$	$n = 15.5$	
$\sigma_2 = 0.011\ [Nmsec/rad]$	Power = 200 [Wats]	

They capture the distributed friction characteristics on the motor. $\mu_0 < 1$ is the friction coefficient of this integrated model[2].

[2]In the LuGre model μ_0 is replaced with the function $g(v) = F_C + (F_S - F_C)e^{(v/v_0)^2}$ (where F_C is the Coulomb friction, F_S is the Sticktion friction level, and v_0 is the Stribeck velocity) in order to include the Stribeck effect. For simplicity reazons, we just use μ_0 which is the Coulomb friction normalized by the Normal force. Since our main objective here is to study the eccentricity effects, we have explicitly introduced the normal force dependency in the LuGre model, and simplified the expression of $g(v)$.

Model (32) can be rewritten as

$$J\dot{v} = u - F - \Lambda\cos(\omega x + \Phi) \tag{35}$$

with

$$F = \left[\frac{F_N}{n} + F_{Nm}\right](\bar{\sigma}_0\eta + \bar{\sigma}_1\dot{\eta} + \bar{\sigma}_2 v) \tag{36}$$

$$= \sigma_0\eta + \sigma_1\dot{\eta} + \sigma_2 v \tag{37}$$

$$\dot{\eta} = v - \frac{\sigma_0|v|}{F_C}\eta; \quad F_C \triangleq \mu_0\left(\frac{F_N}{n} + F_{Nm}\right) \tag{38}$$

$$\omega = \frac{\bar{\omega}}{n} = \frac{2R_0}{n(r+R)} \tag{39}$$

$$\Lambda = k_S\frac{R-r}{2}\cdot\frac{F_N}{n}\nu(\eta,\dot{\eta},v) \tag{40}$$

$$\approx k_S\frac{R-r}{2}\cdot\frac{F_N}{n}\nu_{SS} = k_S\frac{R-r}{2}\cdot\frac{F_N}{n}\mu_0\cdot\text{sign}(v). \tag{41}$$

ω is the dimensionless frequency at the motor side (note that the eccentricity frequency effect at the motor shaft is demultiplied by the gear ratio). Note also that model (35) differs from model (1) by the presence of friction, and by the dependence of Λ on $\nu(\cdot)$. Hence to apply to our previous adaptive eccentricity compensator, we need to cancel the friction, and to assume that $\nu(\eta,\dot{\eta},v)$, can be approximate by its steady-state value $\nu_{SS} = \mu_0\,\text{sign}(v)$, as shown in (41).

Friction can be canceled via feedforward or feedback. The approximation on $\nu(\cdot) \approx \nu_{SS}$ may hold for most operation conditions (except for the time periods when the velocity crosses zero) since the friction dynamics of (34), is much faster than the motor velocity dynamic (of the order of magnitude of $\sigma_0 \approx 10^2$. The only conceptual problem lies thus on the velocity zero crossings that occurs at isolated time periods. Its effects on the closed-loop performance will be evaluated through experiments.

Resuming, we have the following.

- To apply our AEC strategy, we must first compensate for the position-independent friction F.
- The dependency of η and $\dot{\eta}$ on Λ is not a problem since the dynamic of $\eta(t)$ is faster than the one of $x(t)$, and $v(t)$.
- The effects of sign-velocity dependency of Λ on the closed-loop system will not be explicitly considered, but they will be evaluated through experiments.

We are thus in position to apply our control algorithm, and for that we will use our AEC controller, with feedforward compensation

$$u = J\dot{v}_d - H(s)(v - v_d) + \hat{F} - s\cdot\hat{z}_1 \tag{42}$$

where $H(s)$ being a linear operator (when referring to the AEC controller we will simply refer to a proportional velocity gain, i.e., $H(s) = k_v$), $\hat{z}_1$ is given by the set of (27)–(30), and $\hat{F}$ is a feedforward friction prediction obtained from

$$\hat{F} = \sigma_0\hat{\eta} + \sigma_1\dot{\hat{\eta}} + \sigma_2 v_d \tag{43}$$

$$\dot{\hat{\eta}} = v_d - \frac{\sigma_0|v_d|}{\mu_0}\hat{\eta}, \quad \hat{\eta}(0) = 0. \tag{44}$$

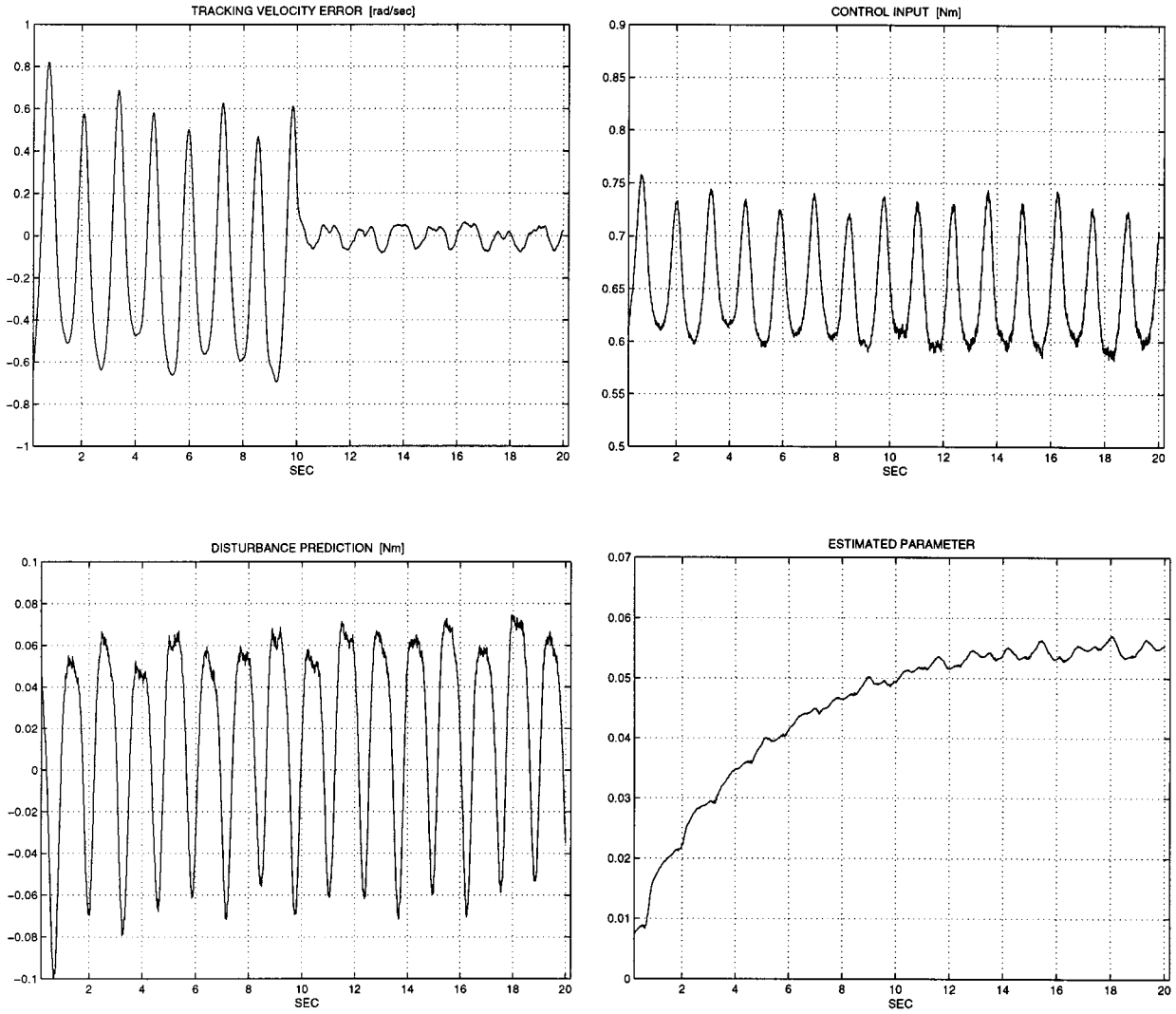

Fig. 5. Experiments under constant velocities $v_d = 30$ Rad/s. Upper left: Velocity tracking error $(v_d - v)$. Upper right: control input time profile. Lower left: predicted disturbance, $\hat{z}_1$. Lower right: time-evolution of $\hat{\theta}(t)$.

Fig. 4 show the block diagram of the EAC control scheme with feedforward friction compensation. Locally, $\hat{F} \approx F$, thus the closed-loop equation with this additional friction compensation term is similar to the frictionless system studied in the previous section.

System parameters including friction coefficients have been estimated using a similar procedure as described in [4]. They are reported in Table I.

The experiments were conducted on a dSPACE real-time computer system based on a digital signal processor, with a sampling time of 1 ms. The position x is measured by means of a high-precision optical encoder of 120 000 divisions, yielding a resolution of 0.52 μrad. The velocity is is computed by position differentiation over a sampling period. The major source of noise is thus caused by the numerical errors due to this approximation.

B. Performance Evaluation under Different Tracking Signals

In this section, we presents several experiments aiming at evaluating the AEC control behavior under different operating conditions: constant velocities, time-varying velocities, and velocity reversals. The control parameters used for these experiments were

- *Controller gains:* $k_v = 40$, $k_P = 50$, $k_I = 400$ (the K_P and K_I, gains are the PI-control gains used later for comparisons.
- *Observer gains:* $k_0 = 1$, $k_1 = 5$.
- *Adaptation gains:* $\gamma = 2$.

1) Experiments Under Constant Velocities: The experiments in Fig. 5, show the tracking error, the prediction $\hat{z}_1(t)$, the estimate $\hat{\theta}$, and the control signal. The experiments are realized at $v_d = 30$ rad/s. The eccentricity compensation is applied at $t = 10$ s. It can be observed that the oscillatory disturbance affecting the tracking error is canceled when applying the term $\hat{z}_1(t)$, in u. The remaining error, which is about 12% of v_d before compensation, is reduced to 1.5% with the compensation. The time-profiles shown in all the presented figures have been low-pass filtered to extract noise.

The time evolution of $\hat{z}_1(t)$, has a shape similar to a sinusoidal wave (as it has been predicted). The imperfections may

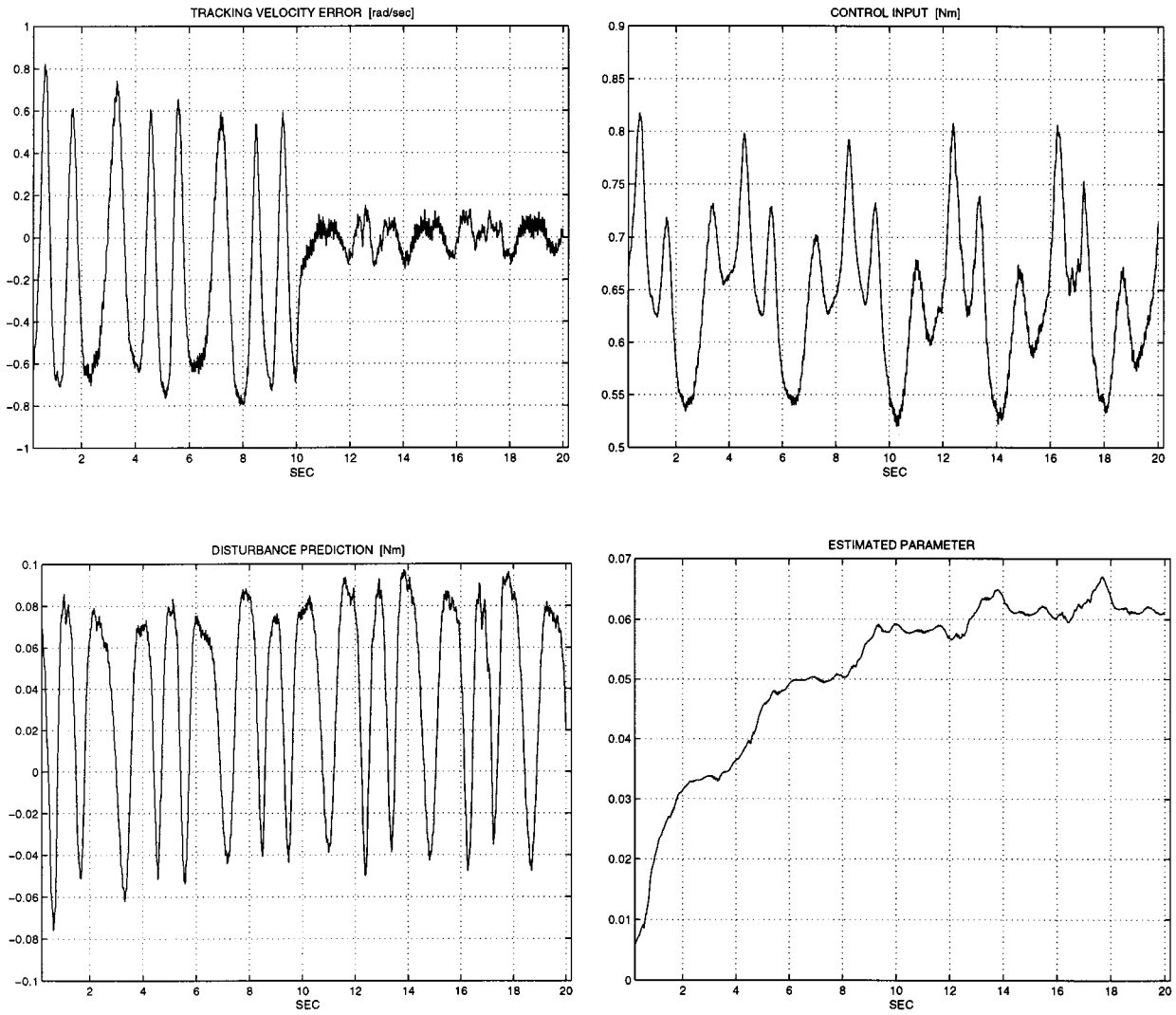

Fig. 6. Experiments under time-varying velocities $v_d = 30 + 10\sin(\pi/2t)$. Upper left: Velocity tracking error $(v_d - v)$. Upper right: control input time profile. Lower left: predicted disturbance, $\hat{z}_1$. Lower right: Time-evolution of $\hat{\theta}(t)$.

be attributed to the nonuniform deformation of the wheel contact surface (the wheel in contact is composed of a inner undeformable steel wheel, covered by a rubber 5 mm o-ring). The estimated parameter $\hat{\theta}$ is observed to converge (in average sense) to a value close to 0.055, which according to two implies that $\omega = \sqrt{0.055} = 0.23$. The theoretical value of ω is given by the expression (39) as $\omega = (2R_0/n(r+R)) = 3/15 = 0.2$, which seems to correspond to the experimental found value (note also that the period of $\hat{z}_1(t)$ gives for a velocity of 30 rad/s, an experimental value of $\omega = (2\pi)/(vT) \approx 0.2$, for a $T = 1.6\pi$).

2) Experiments Under Time-Varying Velocities.: The experiments in Fig. 6, show the tracking error, the prediction $\hat{z}_1(t)$, the estimated value of θ, and the control signal. The experiments are realized under a positive time-varying desired velocity profile $v_d = 30 + 10\sin(\pi/2t)$, under the same AEC controller. Note that the predicted $\hat{z}_1(t)$ does not necessarily resembles to a pure sinusoidal wave. Conceptually, the magnitude Λ of the disturbance $d(x)$, may change (not much) as a function of the velocity (see discussion at the end of Section IV-A) due to the viscous friction term σ_2, in $\mu(\cdot)$, but this seems to have a negligible effect on the closed-loop performance. The main (small) difference with respect to the previous experiment, is a slightly large level of noise. Nevertheless, the global system behavior is preserved. Finally, note that the value of $\hat{\theta}$ tends to a value similar to the one obtained for constant velocity.

C. Comparison Between the AEC and the PI Controllers

The effect of the disturbance $d(x)$ on the output v, in system (1), under a linear controller $u = -H(s)(v - v_d)$, can be quantified by looking at the spectral distribution of sensitivity function $T(s)$, where

$$v = T(s)d, T(s) \triangleq \frac{1}{Js + H(s)}. \tag{45}$$

In this section we compare the AEC-controller $(H(s) = k_v)$, with a simpler PI-controller $(H(s) = k_P + \frac{k_I}{s})$, usually used to regulate velocity. For this comparison to be fair, we set the gains k_v, k_P, and k_I, such that the PI controller have a better rejection characteristics than the P controller (linear part of the AEC), in

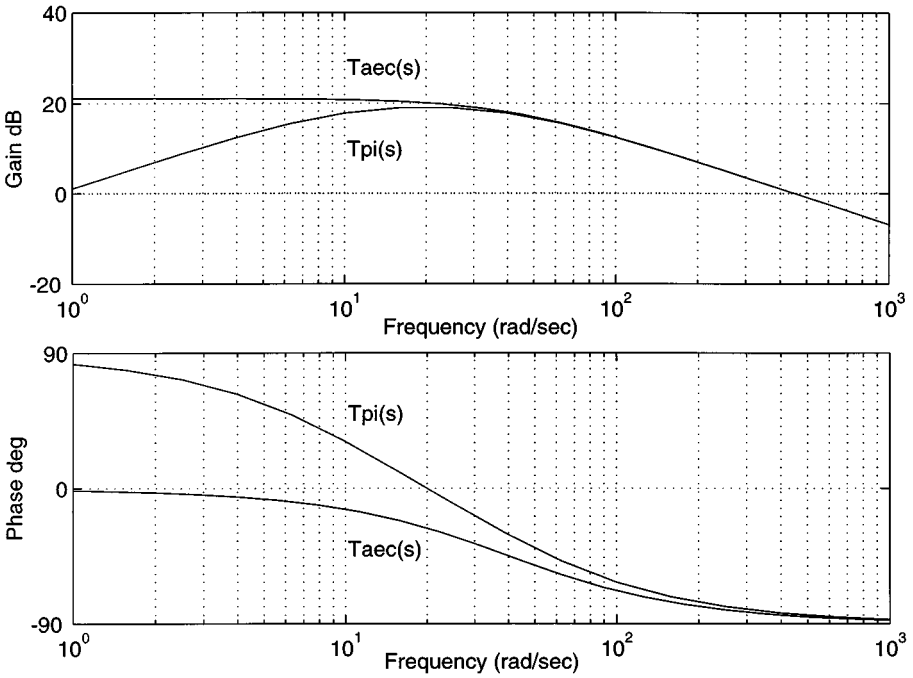

Fig. 7. Bode plots of the sensibility functions: $T_{\mathrm{AEC}}(s)$-AEC controller and $T_{\mathrm{PI}}(s)$-PI controller.

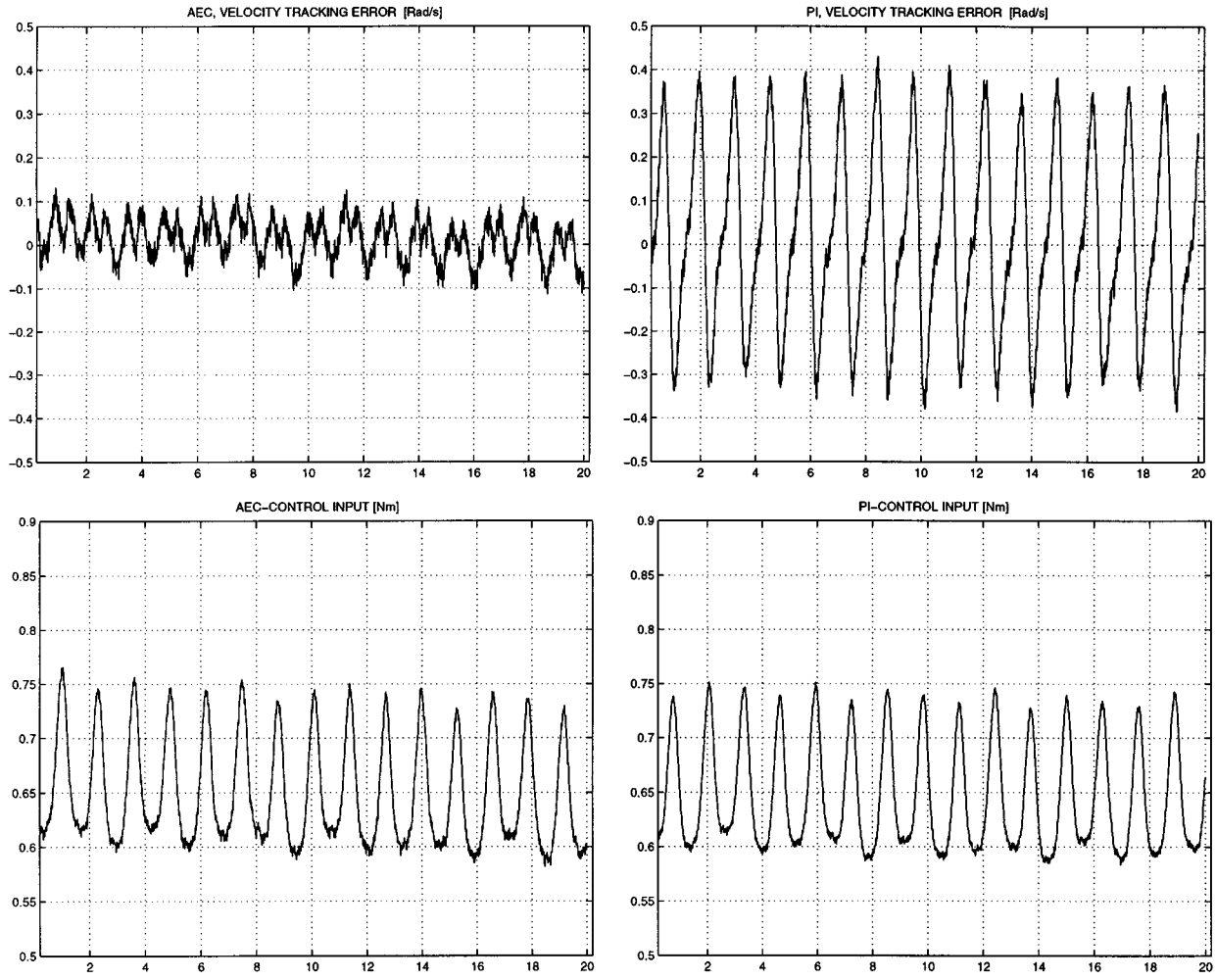

Fig. 8. Comparisons between the AEC and the PI controller. Upper left: velocity tracking error $(v_d - v)$ for the AEC-controller. Upper right: velocity tracking error $(v_d - v)$ for the PI-controller. Lower left: AEC-control input time profile. Lower right: PI-control input time profile.

TABLE II
PERFORMANCE QUANTIFIERS OF THE COMPARISON BETWEEN THE AEC AND THE PI CONTROLLERS UNDER DIFFERENT VELOCITY PROFILES: $v_{d1} = 10$ [rad/s], $v_{d2} = 40$ [rad/s], $v_{d3} = 20 + 10\sin(0.78t)$ [rad/s], AND $v_{d4} = 40 + 10\sin(0.78t)$ [rad/s]

	v_{d1}		v_{d2}		v_{d3}		v_{d4}	
	EAC	PI	EAC	PI	EAC	PI	EAC	PI
Maximum Error: $\|e(t)\|_{\max}$	0.4326	0.2834	0.1452	0.4034	0.1993	0.4204	0.3538	0.5898
Mean error: mean$\|e(t)\|$	0.0792	0.0956	0.0402	0.1836	0.0523	0.1356	0.1039	0.2089
Variance : σ^2	0.0089	0.0134	0.0017	0.0478	0.0041	0.0280	0.0143	0.0614
Maximum signal: $\|u(t)\|_{\max}$	0.5976	0.6190	0.7165	0.7610	0.7454	0.7520	0.8237	0.8312
Integral value: $\int_0^T u(\tau)^2 d\tau$	469	515	765	850	666	665	914	933
Mean value: mean$u(\tau)$	0.4819	0.5054	0.6168	0.6499	0.5726	0.5715	0.6733	0.6802
Variance : σ^2	0.0023	0.0024	0.0024	0.0026	0.0053	0.0061	0.0036	0.0039

the frequency domain where the spectral support of the d is expected to lie, i.e., $|T_{\rm AEC}(j\omega)| > |T_{\rm PI}(j\omega)|\ \forall\omega \in [0, 40R/s]$, and $|T_{\rm AEC}(j\omega)| \approx |T_{\rm PI}(j\omega)|$ elsewhere. Fig. 7 shown the magnitudes of $T_{\rm AEC}(j\omega)$, and $T_{\rm PI}(j\omega)$, with the given choice of parameters.

Fig. 8 shown the tracking error and the control signal for both controllers with $v_d = 40$ rad/s. At this velocity, $d(x(t)) = \Lambda\cos(4.8t+\Phi)$ has its spectrum concentrated at 4.8 rad/s. From Fig. 7, we see that $T_{\rm PI}(j\omega)$ is about 8 dB smaller than the one of the AEC. Although, the performance of the AEC-controller improves over the PI, it may be expected that this improvement will diminish when operating at lower frequencies where $T_{\rm PI}(j\omega)$ is small.

Table II shows several quantifiers (maximum value, mean values, variance, etc.) of the tracking error and the control signal under several different operation velocity profiles; $v_{d1}, v_{d2}, v_{d3}, v_{d4}$ (see table description).

The first two set of trials correspond to constant velocities: one with low velocity and the other with higher velocity. For the low velocity case (v_{d1}), the PI sensibility function $T_{\rm PI}(s)$ has a substantial low magnitude. This is the less favorable case for the AEC-controller. Nevertheless, both controllers performance are comparable. The explicit prediction and compensation of the disturbance replace the need for a low magnitude of the sensitivity function at low frequencies. For larger velocities (i.e., v_{d2}), the AEC-controller overperform the PI controller.

The second set of trials corresponds to time-varying velocity profiles. In some applications it is required to operate under velocity changes. Thus linear controllers tuned for a particular operational velocity, may degrade its performance while confronted to changes in v_d. The experiment concerning the profile v_{d3} produce a change of velocity between ten and 30 rad/s, while the profile v_{d4} produce a change of velocity between 30 and 50 rad/s. From Table II, it can be observed that in all these trials, the AEC controller improves over the PI with equivalent control authority.

V. CONCLUSION

We have presented a method for compensating eccentricity in mechanical systems. As a main difference with previous works, we have formulated the disturbance as a position-dependent periodic function, leading to a velocity-dependent state space representation. This formulation seems to be justified in most of the mechanical applications where eccentricity occurs.

From this formulation, we have designed an adaptive predictor which allows to reject the eccentricity effects studied in this paper. The adaptive eccentricity compensator has been shown to be asymptotically stable while ensuring internal signal boundedness.

We have also presented several experiments of the AEC that demonstrated the improvements over simpler linear controllers (PD and PID). The experiments were conducted under different velocity profiles with different amplitudes. The obtained results have demonstrated that the AEC mechanism improves over the linear controllers. Besides that, and in opposition to some of the existing mechanisms, our AEC do not require any gain retuning when operating at different velocities.

We have also observed that to the internal observer signal to behave well, it was important to compensate for the motor friction. When this was not the case, the additional bias is in the system due to inexact friction cancellation provokes a high-oscillatory behavior on the estimate $\hat{\theta}$ (which can be due to one of the well-known phenomena of drift, bursting, and parameter recovery, see for example [9]). Although, this does not change much the time-profile of z_1, this particular phenomena deserves more attention.

ACKNOWLEDGMENT

The first author would like to thanks P. Posselius and H. Olofsson for their help in performing the experiments and the interesting discussions that resulted during their stay at Grenoble.

REFERENCES

[1] M. Bodson and S. C. Douglas, "Adaptive algorithm for the rejection of periodic disturbances with unknown frequency," *Automatica*, vol. 33, no. 12, pp. 2213–2221, 1997.
[2] M. Bodson, A. Sacks, and P. Khosla, "Harmonic generation in adaptive feedforward cancellation schemes," *IEEE Trans. Automat. Contr.*, vol. 39, pp. 1939–1944, 1994.
[3] C. Canudas de Wit, H. Olsson, K. J. Âström, and P. Lischinsky, "A new model for control of systems with friction," *IEEE Trans. Automat. Contr.*, vol. 40, pp. 419–425, Mar. 1995.
[4] C. Canudas de Wit and P. Lischinsky, "Adaptive friction compensation with partially known dynamic friction model," *Int. J. Adapt. Contr. Signal Process.*, vol. 11, pp. 65–85, 1997.

[5] U. Emborg and C. F. Ross, "Active control in the Saab," in *340 Proc. 2nd Conf. Recent Adv. Active Contr. Sound Vibrations*, Blacksburg, VA, 1993, pp. S67–S73.
[6] L. J. Eriksson, "A practical system for active attenuation in ducts," *Sound Vibr.*, vol. 22, no. 2, pp. 30–40, 1988.
[7] S. S. Garimella and K. Srinivasan, "Application of repetitive control to eccentricity compensation in rolling," *J Dyn. Syst., Meas., Contr.*, vol. 118, pp. 657–664, Dec. 1996.
[8] H. Olofsson and P. Posselius, "Experimental Study of Adaptive Eccentricity Compensation," Lab. Automat. Contr., Grenoble, France, Int. Rep., 1998.
[9] M. España and L. Praly, "On the global dynamics of adaptive systems: A study of an elementary example," *SIAM J. Contr. Optimi.*, vol. 31, no. 5, pp. 1143–1166, Sept. 1993.
[10] R. Shoureshi and P. Knurek, "Automotive application of a hybrid active noise and vibration control," *IEEE Contr. Syst. Mag.*, vol. 16, no. 6, pp. 72–78, 1996.

Carlos Canudas de Wit was born in Villahermosa, Tabasco, Mexico, in 1958. He received the B.Sc. degree in electronics and communications from the Technological Institute of Monterrey, Mexico, in 1980. He received the M.Sc. and Ph.D. degrees in automatic control from the Polytechnic of Grenoble, France, in 1984 and 1987, respectively.

Since 1987, he has been working at the same department as "Directeur de recherche" at the CNRS, where he teaches and conducts research in the area of adaptive and robot control. He is also responsible for a team on control of electromechanical systems and robotics. He teaches undergraduate and graduated courses in robot control and stability of nonlinear systems. He was a Visiting Researcher in 1985 at the Lund Institute of Technology, Sweden. His research topics include adaptive control, identification, robot control, nonlinear observers, control of systems with friction, ac and CD drives, automotive control, and nonholonomic systems. He has written the book *Adaptive Control of Partially Known Systems: Theory and Applications* (Amsterdam, The Netherlands: Elsevier, 1988). He also edited two books, *Advanced Robot Control* (New York: Springer-Verlag, 1991) and *Theory of Robot Control*, in the Springer Control and Communication Series.

Dr. de Wit was Associate Editor of the IEEE TRANSACTIONS ON AUTOMATIC CONTROL from January 1992 to December 1997 and has been Associate Editor of *Automatica* since March 1999.

Laurent Praly received the engineering degree from École Nationale Supérieure des Mines de Paris, France, in 1976.

After working in industry for three years, in 1980 he joined the Centre Automatique et Systèmes at École des Mines de Paris. From July 1984 to June 1985, he spent a sabbatical year as a Visiting Assistant Professor in the Department of Electrical and Computer Engineering, University of Illinois, Urbana-Champaign. Since 1985, he has continued at the Centre Automatique et Systèmes, where he served as Director for two years. In 1993, he spent a quarter at the Institute for Mathematics and its Applications at the University of Minnesota, Minneapolis, where he was an Invited Researcher. His main interest is in feedback stabilization of controlled dynamical systems under various aspects—linear and nonlinear dynamic output, with parametric or dynamic uncertainty. On this topic, he is contributing both on the theoretical aspect with many academic publications and the practical aspect with several industrial applications.